ARTICLE IN PRESS – Acta Cryst. F

STRUCTURAL BIOLOGY COMMUNICATIONS

ISSN 2053-230X

# Conformational changes on substrate binding revealed by structures of *Methylobacterium extorquens* malate dehydrogenase

## Proof instructions

Proof corrections should be returned by **9 September 2018**. After this period, the Editors reserve the right to publish your article with only the Managing Editor's corrections.

Please
(1) Read these proofs and assess whether any corrections are necessary.
(2) Check that any technical editing queries highlighted in **bold underlined** text have been answered.
(3) Send corrections by e-mail to **lj@iucr.org**. Please describe corrections using plain text, where possible, giving the line numbers indicated in the proof. Please do not make corrections to the pdf file electronically and please do not return the pdf file. If no corrections are required please let us know.

To arrange payment for **open access**, please visit **http://shop.iucr.org/iucrshop/viewitem/openaccess/?code=rf5009**. To purchase printed offprints, please complete the attached order form and return it by e-mail.

## Please check the following details for your article

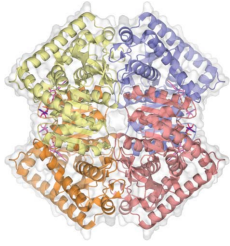

**Thumbnail image for contents page**

**Synopsis:** The structure of *M. extorquens* malate dehydrogenase is reported, together with an analysis of structural rearrangements on substrate binding.

**Abbreviated author list:** González, J.M. (0000-0002-3298-2235); Marti-Arbona, R. (0000-0002-9720-977X); Chen, J.C.-H.; Broom-Peltz, B.; Unkefer, C.J. (0000-0002-9263-3221)

**Keywords:** malate dehydrogenase; methylotrophs; biofuels; *Methylobacterium extorquens*



## How to cite your article in press

Your article has not yet been assigned page numbers, but may be cited using the doi:

González, J.M., Marti-Arbona, R., Chen, J.C.-H., Broom-Peltz, B. & Unkefer, C.J. (2018). *Acta Cryst.* F**74**, https://doi.org/10.1107/S2053230X18011809.

You will be sent the full citation when your article is published and also given instructions on how to download an electronic reprint of your article.

Acta Cryst F
STRUCTURAL BIOLOGY COMMUNICATIONS
ISSN 2053-230X

# Conformational changes on substrate binding revealed by structures of *Methylobacterium extorquens* malate dehydrogenase

Javier M. González,[a] Ricardo Marti-Arbona,[b]* Julian C.-H. Chen,[b] Brian Broom-Peltz[b] and Clifford J. Unkefer[b]*

[a]Instituto de Bionanotecnología del NOA, Consejo Nacional de Investigaciones Científicas y Técnicas, Universidad Nacional de Santiago del Estero, G4206XCP Santiago del Estero, Argentina, and [b]Bioscience Division, Los Alamos National Laboratory, Los Alamos, NM 87544, USA. *Correspondence e-mail: rm-a@lanl.gov, cju@lanl.gov

Received 2 May 2018
Accepted 20 August 2018

Edited by S. Sheriff, Bristol-Myers Squibb, USA

**Keywords:** malate dehydrogenase; methylotrophs; biofuels; *Methylobacterium extorquens*.

**PDB references:** malate dehydrogenase from *M. extorquens*, 5ulv; complex with oxaloacetate and adenosine 5-diphosphoribose, 4ros; complex with NAD$^+$, 5ujk

**Supporting information:** this article has supporting information at journals.iucr.org/f

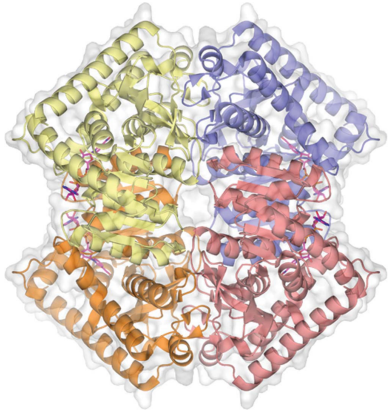



Three high-resolution X-ray crystal structures of malate dehydrogenase (MDH; EC 1.1.1.37) from the methylotroph *Methylobacterium extorquens* AM1 are presented. By comparing the structures of apo MDH, a binary complex of MDH and NAD$^+$, and a ternary complex of MDH and oxaloacetate with ADP-ribose occupying the pyridine nucleotide-binding site, conformational changes associated with the formation of the catalytic complex were characterized. While the substrate-binding site is accessible in the enzyme resting state or NAD$^+$-bound forms, the substrate-bound form exhibits a closed conformation. This conformational change involves the transition of an $\alpha$-helix to a $3_{10}$-helix, which causes the adjacent loop to close the active site following coenzyme and substrate binding. In the ternary complex, His284 forms a hydrogen bond to the C2 carbonyl of oxaloacetate, placing it in a position to donate a proton in the formation of (2*S*)-malate.

## 1. Introduction

Malate dehydrogenase (MDH; EC 1.1.1.37) reversibly catalyzes the reduction of oxaloacetate to (2*S*)-malate using NADH as a reductant. It is a member of the lactate dehydrogenase-like family, which primarily includes lactate dehydrogenases (EC 1.1.1.27) and malate dehydrogenases (EC 1.1.1.37) (Zarzycki & Kerfeld, 2013). In aerobic organisms, MDH plays a central role in energy generation as part of the citric acid cycle, where it primarily functions in the oxidation of malate. However, during the growth of the methylotroph *Methylobacterium extorquens* AM1 on $C_1$ compounds, MDH functions in the *icl*$^-$-serine pathway for formaldehyde assimilation (Anthony, 1982). During growth on methanol as its sole carbon source, *M. extorquens* AM1 derives its energy from the pyrroloquinoline quinone-dependent methanol dehydrogenase-catalyzed oxidation of methanol, yielding formaldehyde. Formaldehyde, as 5,10-methylene tetrahydrofolate, is condensed with glycine *via* serine hydroxymethyltransferase. MDH functions in the serine pathway, which provides glyoxylate for the regeneration of glycine. In contrast to its role in the TCA cycle, in the *icl*$^-$-serine pathway MDH primarily functions in the reduction of oxaloacetic acid.

The lactate/malate dehydrogenase family is well represented in the Protein Data Bank (PDB). The members of this family contain an NAD$^+$-binding domain with a characteristic Rossmann fold (Rao & Rossmann, 1973) of the form $(\beta\alpha\beta)_2(\alpha\beta)_2$. Structural studies have shown that substrate binding causes a conformational change around the active site, in which a mobile loop closes to bring key residues into

**Table 1**
Macromolecule-production information.

| | |
|---|---|
| Source organism | *M. extorquens* AM1 |
| DNA source | Synthetic, Genewiz |
| Forward primer | N/A |
| Reverse primer | N/A |
| Cloning vector | pET-42a(+), Novagen |
| Expression vector | pET-42a(+), Novagen |
| Expression host | *E. coli* (DE3) ArcticExpress, Stratagene |
| Complete amino-acid sequence of the construct produced | MARSKIALIGAGQIGGTLAHLAGLKELGDV VLFDIVDGVPQGKALDIAESAPVDGFDA KYSGASDYSAIAGADVVIVTAGVPRKPG MSRDDLIGINLKVMEAVGAGIKEHAPDA FVICITNPLDAMVWALQKFSGLPTNKVV GMAGVLDSARFRHFLAEEFGVSVEDVTA FVLGGHGDDMVPLTRYSTVAGVPLTDLV KLGWTTQEKLDAMVERTRKGGGEIVNLL KTGSAFYAPAASAIAMAESYLRDKKRVL PCAAYLDGQYGIDGLYVGVPVVIGENGV ERVLEVTFNDDEKAMFEKSVNSVKGLIE ACKSVNDKLAHHHHHHHH |

contact with the substrate (Chapman *et al.*, 1999). Here, we report three high-resolution structures of *M. extorquens* AM1 MDH: uncomplexed, with $NAD^+$ bound and with ADP-ribose occupying the $NAD^+$-binding site and oxaloacetate occupying the substrate site.

## 2. Materials and methods

### 2.1. Macromolecule production

**2.1.1. Materials.** Unless otherwise noted, all chemicals were obtained from Sigma–Aldrich. Oligonucleotide-synthesis and DNA-sequencing reactions were performed by Genewiz. The pET-42a(+) expression vector (Novagen) and ArcticExpress (DE3) competent *Escherichia coli* cells (Stratagene) were obtained from commercial sources.

**2.1.2. Cloning of *Mex*MDH.** A gene encoding malate dehydrogenase from *M. extorquens* AM1 with codons optimized for expression in *E. coli* was synthesized and subcloned into pET-42a(+) by Genewiz. The NdeI and XhoI cloning sites were used to obtain a clone that expressed *Mex*MDH with a $His_8$ tag at the C-terminus of the protein (*Mex*MDH-$His_8$; Table 1).

### 2.2. Protein expression and purification

*E. coli* ArcticExpress (DE3) competent cells transformed with expression vector encoding *Mex*MDH-$His_8$ were selected by growth on an LB–agar plate containing 50 µg $ml^{-1}$ kanamycin. A single colony was cultured overnight (at 37°C on a rotary shaker) in 25 ml LB medium containing 50 µg $ml^{-1}$ kanamycin. 4 ml of this culture was then used to inoculate 2 l LB medium containing 50 µg $ml^{-1}$ kanamycin. The cells were cultured (at 37°C on a rotary shaker) until an $OD_{600}$ of 0.6 was reached. The temperature of the culture was lowered to 16°C, isopropyl β-D-1-thiogalactopyranoside (IPTG; 238 mg $l^{-1}$) was added to a final concentration of 1 m*M* to induce expression and the culture was incubated overnight. Bacterial cells were harvested by centrifugation at 7000*g* for 10 min at 4°C. The pellet was washed and resuspended (10 ml per gram of cells) in 20 m*M* sodium phosphate buffer containing 50 m*M* NaCl and 5 m*M* imidazole pH 7.4 (buffer *A*). Before cell disruption, 5 µg $ml^{-1}$ DNAse and 0.1 mg $ml^{-1}$ of the protease inhibitor phenylmethylsulfonyl fluoride were added to the cell suspension. The cell suspension was cooled using an ice bath and lysed by sonication (Cole Palmer Sonic Processor). Using an amplitude of 95%, the sonicator was cycled 2 s on followed by 2 s off for a total of 10 min. The sample was then cooled for 5 min. This sonication cycle was carried out a total of three times. The soluble protein was separated from the cell debris by centrifugation at 12 000*g* for 15 min at 4°C and was then loaded onto two 5 ml HisTrap columns (GE Healthcare) connected in tandem and equilibrated with buffer *A*. *Mex*MDH-$His_8$ was eluted with a linear gradient of buffer *A* and 500 m*M* imidazole pH 7.4 (buffer *B*). Fractions containing *Mex*MDH-$His_8$ were pooled, concentrated, loaded onto a HiLoad 26/60 Superdex 200 prep-grade gel-filtration column (GE Healthcare) and eluted with 20 m*M* HEPES buffer, 50 m*M* NaCl pH 7.2 (buffer *C*). The purity of the protein was monitored by SDS gel electrophoresis. The protein concentration was estimated from the $A_{280}$ using a theoretical extinction coefficient of 0.64 mg $ml^{-1}$ $cm^{-1}$ calculated using the protein identification and analysis tools on the *ExPASy* server.

**Table 2**
Crystallization.

| | |
|---|---|
| Method | Vapor diffusion, sitting drop |
| Plate type | 96-well Intelli-Plate, 24-well VDX |
| Temperature (K) | 298 |
| Protein concentration (mg $ml^{-1}$) | 20 |
| Buffer composition of protein solution | 10 m*M* HEPES pH 8.0, 20 m*M* NaCl |
| Composition of reservoir solution | 0.1 *M* HEPES pH 7.5, 25–28% PEG 400, 180–220 m*M* $CaCl_2$ |
| Volume and ratio of drop | 4 µl, 1:1 |
| Volume of reservoir (µl) | 1000 |

### 2.3. Protein characterization

**2.3.1. Protein molecular-weight determination.** A Tricorn 5/150 column (GE Healthcare) was packed with Superdex 200 prep-grade resin and equilibrated with buffer consisting of 50 m*M* Tris, 50 m*M* NaCl pH 8.0. The column was calibrated with a gel-filtration markers kit for protein molecular weights 12–200 000 kDa (Sigma–Aldrich). To determine the elution volumes for each of the protein standards and for *Mex*MDH-$His_8$, the proteins were diluted in equilibration buffer to a final concentration of 1 mg $ml^{-1}$. 100 µl of each protein solution was loaded onto the column. The size of purified *Mex*MDH-$His_8$ was then estimated using a calibration curve prepared by plotting the molecular weights of the protein standards *versus* their elution volumes.

**2.3.2. Specific activity determination.** The specific activity of MDH for the reduction of oxaloacetate to malate was monitored spectrophotometrically at 340 nm by following the oxidation of NADH using a Synergy H4 hybrid microplate reader (BioTek Instruments). The standard assay consisted of 100 m*M* HEPES pH 8.1, 100 m*M* KCl, 0.1 mg $ml^{-1}$ BSA,

**Table 3**
Data collection and processing.

Values in parentheses are for the outer shell.

| | Apo *Mex*MDH | *Mex*MDH–OAA/APR | *Mex*MDH–$NAD^+$ |
|---|---|---|---|
| Diffraction source | BL7-1, SSRL | BL7-1, SSRL | 08ID-1, CLSI |
| Wavelength (Å) | 1.12709 | 1.12709 | 0.97949 |
| Temperature (K) | 100 | 100 | 100 |
| Detector | ADSC Quantum 315R | ADSC Quantum 315R | Rayonix MX-300 |
| Crystal-to-detector distance (mm) | 200 | 250 | 200 |
| Rotation range per image (°) | 0.3 | 0.4 | 0.25 |
| Total rotation range (°) | 102 | 74 | 210 |
| Exposure time per image (s) | 0.5 | 0.5 | 0.6 |
| Space group | $P6_422$ | $P6_422$ | $P6_422$ |
| $a = b$, $c$ (Å) | 108.99, 104.66 | 108.40, 104.01 | 108.19, 104.32 |
| $\alpha = \beta$, $\gamma$ (°) | 90, 120 | 90, 120 | 90, 120 |
| Mosaicity (°) | 0.17 | 0.20 | 0.58 |
| Resolution range (Å) | 37.75–1.66 (1.72–1.66) | 37.53–1.95 (2.00–1.95) | 54.09–1.53 (1.56–1.53) |
| Total No. of reflections | 494660 (12815) | 218344 (9435) | 580319 (23920) |
| No. of unique reflections | 44052 (2137) | 26510 (1665) | 54696 (2651) |
| Completeness (%) | 99.6 (93.1) | 99 (90) | 100 (99.8) |
| Multiplicity | 11.2 (6.0) | 8.2 (5.7) | 10.6 (9.0) |
| $\langle I/\sigma(I)\rangle$ | 14.2 (2.2) | 23.0 (2.1) | 12.1 (2.2) |
| $R_{meas}$ | 0.092 (0.329) | 0.065 (0.812) | 0.108 (1.088) |
| $CC_{1/2}$ | 0.998 (0.947) | 0.999 (0.711) | 0.998 (0.733) |
| Overall $B$ factor from Wilson plot ($Å^2$) | 18 | 32 | 15 |

0.64 m*M* NADH, 8.0 ng $ml^{-1}$ *Mex*MDH and oxaloacetate in a final volume of 250 µl at 30°C.

**2.3.3. Data analysis**. The kinetic parameters $k_{cat}$ and $K_m$ were determined by fitting the initial velocity data to the Michaelis–Menten model, $v/E_t = k_{cat}A/(K_m + A)$, where $v$ is the initial velocity, $E_t$ is the enzyme concentration, $k_{cat}$ is the turnover number, $A$ is the substrate concentration and $K_m$ is the Michaelis constant.

## 2.4. Crystallization

Crystals of *Mex*MDH were grown using the sitting-drop vapor-diffusion method in 3-well Intelli-Plate 96 trays from Art Robbins Instruments (Table 2). Drops were prepared with an Oryx8 liquid-handling robot (Douglas Instruments). Initial crystallization trials used the commercial screens MCSG-1, MCSG-2, MCSG-3 and MCSG-4 (Midwest Center for Structural Genomics, Microlytic). Crystals appeared after 3–4 d of incubation at 298 K in a medium corresponding to condition No. 10 of the MCSG-1 crystallization screen. Crystals were successfully reproduced in 24-well VDX plates in a sitting-drop setup with micro-bridges (Hampton) using the conditions described in Table 2 (Supplementary Fig. S1). In general, *Mex*MDH crystals exhibited good diffraction quality, experiencing only minor damage during the ligand-soaking steps, which led to increased mosaicity values. The crystals were mounted in nylon loops (Hampton Research) and flash-cooled in liquid nitrogen; they were cryoprotected in the mother liquor diluted with glycerol to a final concentration of 20%. Complexes of *Mex*MDH with oxaloacetate (OAA) and adenosine 5-diphosphoribose (APR) and with $NAD^+$ were obtained by soaking crystals for 1 h in 1 m*M* ligand solutions by dilution of 100 m*M* stock solutions into the mother liquor. Crystals of *Mex*MDH with OAA and APR appeared fortuitously while attempting to obtain a complex with OAA and $NAD^+$, *i.e.* with both substrate and cofactor oxidized, to prevent the redox reaction from taking place during crystallization. Instead, our sample of $NAD^+$ contained a significant amount of APR which bound in place of $NAD^+$. The fact that APR is the product of the hydrolysis of pyridine dinucleotides and is present in many commercial preparations of $NAD^+$ has been known for many years (Colowick & Kaplan, 1957; Dalziel, 1962*a*). In addition, APR has been shown to be a competitive inhibitor of pyridine nucleotide-dependent dehydrogenases (Dalziel, 1962*a*,*b*).

## 2.5. Data collection and processing

Diffraction data for *Mex*MDH in its apo and OAA/APR-bound forms were collected on beamline BL7-1 of the Stanford Synchrotron Radiation Light Source (SSRL) at a wavelength of 1.127 Å using a ADSC 315r CCD detector (Cohen *et al.*, 2002; Soltis *et al.*, 2008), whereas the *Mex*MDH–$NAD^+$ complex data were collected on beamline 08ID-1 at the Canadian Light Source (CLSI) at a wavelength of 0.9795 Å using a Rayonix MX-300 detector. Reflections were indexed and integrated with *XDS* (Kabsch, 2010). Scaling was performed with *AIMLESS* (Evans & Murshudov, 2013), including structure-factor calculation with the French and Wilson algorithm as implemented in *TRUNCATE* (French & Wilson, 1978) and space-group determination with *POINTLESS* (Evans, 2006). Data-collection and quality statistics are summarized in Table 3.

## 2.6. Structure solution and refinement

The malate/lactate dehydrogenase from *Brucella melitensis* (PDB entry 3gvh; Seattle Structural Genomics Center for Infectious Disease, unpublished work) was used as an initial model for molecular replacement with *Phaser* (McCoy *et al.*, 2007), from which all noncovalently bound ligands, alternate

**Table 4**
Structure solution and refinement.

Values in parentheses are for the outer shell.

| | Apo *Mex*MDH | *Mex*MDH–OAA/APR | *Mex*MDH–NAD$^+$ |
|---|---|---|---|
| PDB code | 5ulv | 4ros | 5ujk |
| Resolution range (Å) | 37.75–1.66 (1.69–1.66) | 34.70–1.95 (2.00–1.95) | 93.69–1.53 (1.57–1.53) |
| No. of reflections | | | |
| Working set | 41822 (2872) | 25164 (1654) | 51855 (3766) |
| Test set | 2191 (176) | 1307 (92) | 2774 (195) |
| Final $R_{cryst}$ | 0.139 (0.203) | 0.168 (0.236) | 0.124 (0.211) |
| Final $R_{free}$ | 0.168 (0.240) | 0.199 (0.280) | 0.177 (0.275) |
| Cruickshank DPI (Å) | 0.070 | 0.120 | 0.060 |
| Polypeptide chains per asymmetric unit | 1 | 1 | 1 |
| No. of non-H atoms | | | |
| Total | 2776 | 2515 | 2676 |
| Protein | 2417 | 2341 | 2336 |
| Ligands | | 45 [OAA, APR] | 46 [NAD$^+$] |
| Ions | 2 [$Ca^{2+}$] | 1 [$Ca^{2+}$] | 2 [$Ca^{2+}$, $Cl^-$] |
| Water molecules | 357 | 127 | 292 |
| R.m.s. deviations | | | |
| Bonds (Å) | 0.020 | 0.019 | 0.019 |
| Angles (°) | 1.9 | 1.9 | 1.8 |
| Average *B* factors (Å$^2$) | | | |
| Overall | 22 | 37 | 25 |
| Protein | 21 | 37 | 24 |
| Ligands | | 36 | 20 |
| Ions | 29 | 49 | 28 |
| Water | 30 | 38 | 32 |
| Ramachandran plot | | | |
| Most favored (%) | 98 | 97 | 98 |
| Allowed (%) | 2 | 3 | 2 |

conformers and solvent molecules were removed. Prior to refinement, the atoms were subjected to a random shift of 0.3 Å to minimize model bias. Structure refinement was performed with *REFMAC*5 (Murshudov *et al.*, 2011) and the *CCP*4 suite of programs (Winn *et al.*, 2011). Manual building was conducted with *Coot* (Emsley *et al.*, 2010) using $\sigma_A$-weighted $2F_o - F_c$ and $F_o - F_c$ Fourier difference maps. Structure validation was performed with *SFCHECK* (Vaguine *et al.*, 1999) and the built-in functions implemented in *Coot*, including the Ramachandran 'most favored' and 'allowed' categories reported in Table 4. The structure of apo *Mex*MDH was then used to phase the structures of the *Mex*MDH–ligand complexes. In all cases (NAD$^+$, OAA and APR) the ligands were clearly discernible in $F_o - F_c$ difference Fourier maps as strong positive density peaks. All ligands were refined in fully occupied sites and displayed *B* factors that were lower than the average for the corresponding proteins. The final models were refined to 1.66, 1.95 and 1.53 Å resolution for apo, OAA/APR-bound and NAD$^+$-bound *Mex*MDH, respectively (Table 4). The refined structures have been deposited in the PDB as entries 5ulv (apo), 4ros (OAA/APR-bound) and 5ujk (NAD$^+$ bound). Figures were prepared with *PyMOL* v.1.2 (Schrödinger) and *CorelDraw* X7.

### 2.7. Phylogenetic analysis of MDH-like proteins

The *Mex*MDH structure (PDB entry 5ulv) and its sequence (UniProt entry A9W386) were used to compare *Mex*MDH with all homologous protein structures available in the PDB. A structure-based search conducted with the *DALI* server (Holm & Rosenström, 2010) using the structure with PDB code 5ulv as a query yielded 145 homologous proteins, which were subsequently reduced to 57 proteins using a 90% identity cutoff. The resulting set of 57 PDB entries was used to map and retrieve the corresponding amino-acid sequences from the UniProtKB database (The UniProt Consortium, 2017). These sequences were then aligned with *ProbCons* (Do *et al.*, 2005) running on the CIPRES computing server (Miller *et al.*, 2010). The resulting multiple sequence alignment was edited with *Jalview* (Waterhouse *et al.*, 2009) to remove highly gapped columns and was used to calculate a maximum-likelihood phylogenetic tree with *RAxML* (Stamatakis, 2014) running on the CIPRES computing server. The best-scoring tree resulted from 708 automatic bootstrap replicates and was used to define three major clades among all MDH-like proteins of known three-dimensional structure. Phylogenetic and alignment results are summarized in Supplementary Figs. S2 and S3.

## 3. Results and discussion

### 3.1. Molecular-weight determination and kinetics

*Mex*MDH-His$_8$ was purified to homogeneity, with a single band visible on the SDS gel aligned with the soybean trypsin inhibitor (32.5 kDa) band of the Kaleidoscope prestained standards, which compares favorably with the predicted molecular weight of 34.7 kDa based on the protein sequence and calculated using the online *PROTEIN CALCULATOR* v.3.4 tool (http://protcalc.sourceforge.net/). The kinetic parameters for *Mex*MDH-His$_8$ were calculated using the decrease in absorbance caused by the enzymatic oxidation of NADH to NAD$^+$ ($\varepsilon$ = 6.22 m$M^{-1}$ cm$^{-1}$) in the presence of oxaloacetate. We obtained a Michaelis constant ($K_m$) of 36.8 $\pm$ 0.6 $\mu M$ for oxaloacetate, which compares favorably to a serine-type methanotroph (Rozova *et al.*, 2015) and is twofold to tenfold lower then those observed for MDHs found in many aerobic bacteria (Rozova *et al.*, 2015; Takahashi-Íñiguez *et al.*, 2016). *Mex*MDH catalyzes the reduction of oxaloacetic acid with a $k_{cat}$ of (4.6 $\pm$ 0.1) $\times$ 10$^2$ s$^{-1}$, yielding a specificity constant $k_{cat}/K_m$ of (1.3 $\pm$ 0.3) $\times$ 10$^7$ $M^{-1}$ s$^{-1}$.

### 3.2. Overall structure

*Mex*MDH rendered hexagonal crystals with symmetry consistent with space group $P6_422$, with one polypeptide chain per asymmetric unit. The structure of *Mex*MDH displays the typical fold of proteins belonging to the lactate dehydrogenase (LDH)/malate dehydrogenase (MDH)-like family (CDD accession cl17195), which contains mostly dimeric and tetrameric 2-hydroxycarboxylic acid dehydrogenases (Marchler-Bauer *et al.*, 2017). Based on calculations using the *PISA* server, *Mex*MDH is stable as a 137.4 kDa tetramer with a buried surface area of 14 740 Å$^2$, which is in agreement with our phylogenetic analysis, where *Mex*MDH belongs to a clade of tetrameric MDH/LDH-like proteins (Supplementary Fig.

S2). Residues 1–143 in the N-terminal domain comprise a characteristic Rossmann fold (Rao & Rossmann, 1973) of the form $(\beta\alpha\beta)_2(\alpha\beta)_2$, which harbors the $NAD^+$-binding site (Fig. 1, Supplementary Fig. S4). The substrate-binding site is located at the interface between this domain and the remainder of the polypeptide (residues 144–320 in the C-terminus).

$NAD^+$ binding induces minor conformational changes, mostly in the flexible loop between $\beta4$ and $\alpha3$ which connects the two Rossmann-fold $\beta\alpha\beta$ motifs. Three specific interactions occur upon $NAD^+$ binding: (i) the 2′- and 3′-OH groups in the adenosine ribose moiety hydrogen-bond to the carboxylate of Asp34, (ii) the backbone carbonyl O atom of Met144 accepts a hydrogen bond from the $NAD^+$ carboxamide amino group and (iii) the O atom of the $NAD^+$ carboxamide carbonyl group accepts a hydrogen bond from His176 protonated at $N^{\varepsilon2}$ (Fig. 2*a*).

In an attempt to obtain a ternary complex of the protein with OAA and $NAD^+$, we performed a soaking procedure as described in §2. Unexpectedly, our solution contained adenosine 5-diphosphoribose (APR) that resulted from hydrolysis of the nicotinamide moiety from $NAD^+$ and led to a *Mex*MDH structure modeled with bound OAA and APR, as shown by the corresponding electron-density maps (Fig. 2*a*). The conformation and identity of each ligand was validated using model-independent isomorphous difference Fourier maps. Given the isomorphism of *Mex*MDH crystals in the apo, $NAD^+$-bound and OAA/APR-bound forms, we constructed Fourier synthesis maps ($\rho_{\rm LIGAND}$) using observed structure-factor differences between the ligand-bound ($F_{\rm LIGAND}$) and apo ($F_{\rm APO}$) refined structures as coefficients and phases calculated from the refined apo structure ($\alpha_{\rm APO}$); that is, $\rho_{\rm LIGAND} = \sum_{hkl}[(F_{\rm LIGAND} - F_{\rm APO}\exp(i\alpha_{\rm APO})]$. By using calculated phases for the apo *Mex*MDH structure, the resulting difference Fourier maps are not biased by the ligand models, thereby providing strong experimental evidence supporting the refined position and conformation of each ligand (Fig. 2*b*).

In contrast to the $NAD^+$-binding scenario, significant conformational changes take place upon OAA binding. While the enzyme resting state and $NAD^+$-bound forms display a structurally similar conformation, the substrate-bound form exhibits a closed conformation. In particular, the $\alpha$-helical segment SRDDLIG in helix $\alpha3$ (residues 88–94) transitions into a $3_{10}$-helix upon substrate binding which, along with the adjacent loop between $\beta4$ and $\alpha3$ (L$\beta4\alpha3$), functions as a door that closes the active site following entrance of the coenzyme and substrate (Fig. 3, Supplementary Fig. S5). Three arginine residues form salt bridges to OAA: Arg152, the conformation of which is minimally changed compared with the apo and $NAD^+$-bound forms, Arg83 in helix $\alpha3$ and Arg89 in L$\beta4\alpha3$ (Fig. 2*b*). The electron densities of the Arg83 and Arg89 side chains are only discernible when the substrate is bound, highlighting their crucial role in stabilizing the negatively charged substrate in the proper orientation. To confirm the model in the SRDDLIG and GGHG regions, we calculated polder OMIT maps (Liebschner *et al.*, 2017), which avoid the artifacts that arise in solvent-exposed regions in traditional OMIT maps (Bhat, 1988). The polder OMIT maps fully support the modeled coordinates, since the SRDDLIG and GGHG regions are clearly discernible in these maps as well as in $2F_{\rm o} - F_{\rm c}$ maps (Supplementary Fig. S6).

The second region affected by substrate binding is the GGHG loop harboring the conserved residue His176 (residues 174–177). As mentioned above, the His176 side chain hydrogen-bonds to the carboxamide carbonyl group of the $NAD^+$ nicotinamide group. However, this interaction is disrupted upon the binding of OAA, which becomes

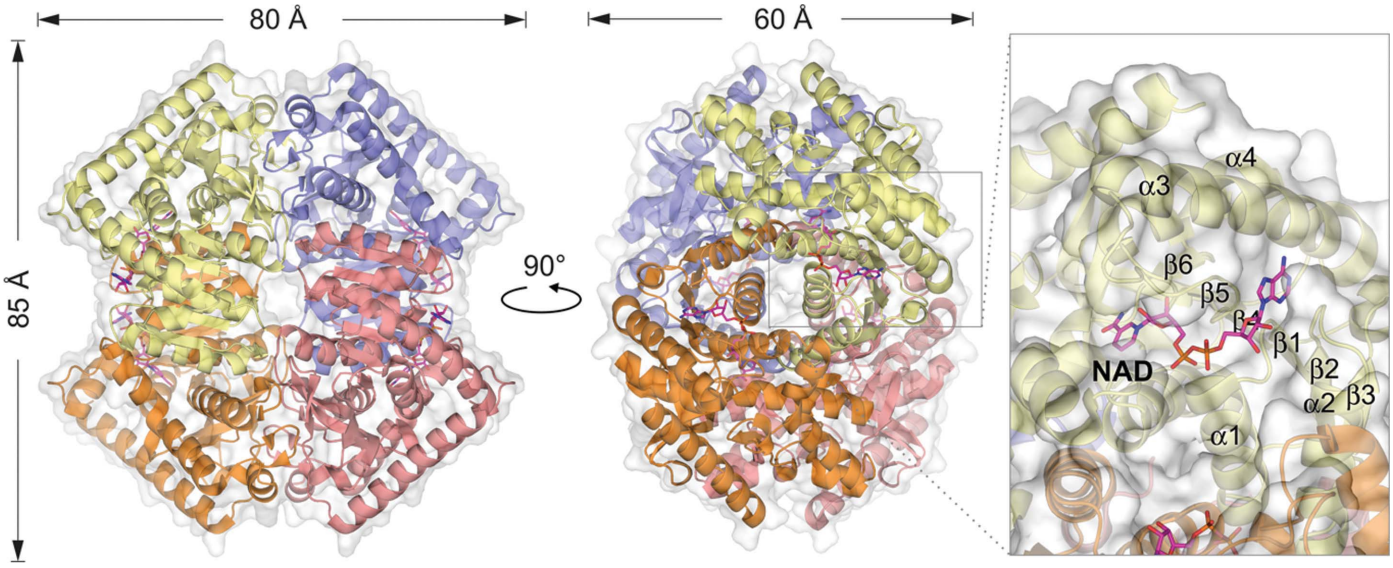


**Figure 1**
Overall structure of *Mex*MDH. The polypeptide displays a Rossmann fold of the form $(\beta\alpha\beta)_2(\alpha\beta)_2$, typical of $NAD^+$-binding MDH/LDH-like proteins; the protein is arranged into a tetramer with one active site per monomer. The figure displays the *Mex*MDH–$NAD^+$ complex as obtained in this work (PDB entry 5ujk).

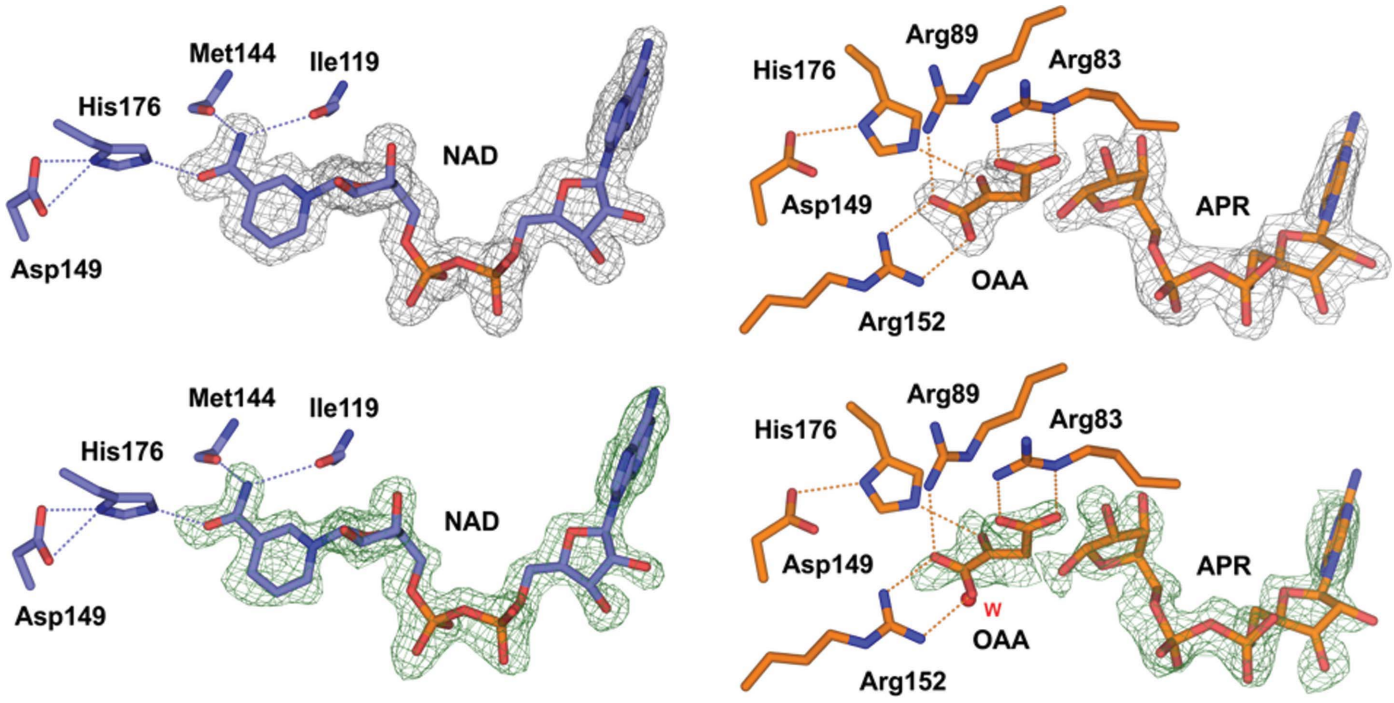


**Figure 2**
Binding of $NAD^+$ and of OAA and APR by *Mex*MDH. (*a*) The carboxamide group of $NAD^+$ (blue) appears to be hydrogen-bonded to the Met144 and Ile119 backbone carbonyls through its amino group, and to the protonated His176 at $N^{\varepsilon 2}$ through its carbonyl O atom. The Asp149 carboxylate also appears to be hydrogen-bonded to the protonated His176 at $N^{\delta 1}$. (*b*) Binding of OAA and APR (orange) induces a significant reorganization of the active site. In the presence of OAA His176 becomes hydrogen-bonded to the carbonyl O atom of OAA, whereas three arginine residues become salt-bridged to OAA carboxylate groups, namely Arg152, Arg83 and Arg89. Wireframe mesh surfaces in the top panels (gray) indicate $2F_o - F_c$ electron-density maps contoured at $1.5\sigma$ and the bottom panels (green) show isomorphous $F_{LIGAND} - F_{APO}$ Fourier difference maps around $NAD^+$ (contoured at $-3.0\sigma$) and OAA/APR (contoured at $-2.0\sigma$). Note that a water molecule 'w' (red) in the apo *Mex*MDH structure is located in a similar position to that of the OAA carboxylate coordinating Arg152, leading to a discontinuity in the corresponding isomorphous difference map. Mechanistically relevant hydrogen-bond interactions are depicted as dashed lines.

hydrogen-bonded to His176 $N^{\varepsilon 2}$ through its own carbonyl group, setting the stage for its protonation and release as malate. The presence of several glycine residues in the GGHG loop undoubtedly enables this conformational change, providing conformational flexibility with minimal energetic costs.

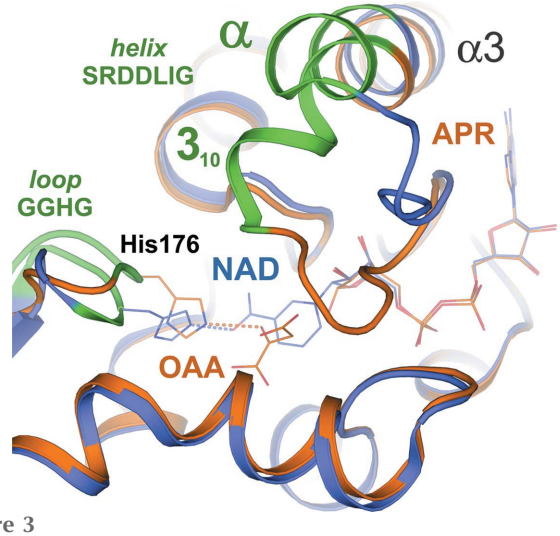


**Figure 3**
Cartoon representation of secondary-structure matching superposition of the structures of *Mex*MDH in the $NAD^+$-bound (blue) and OAA/APR-bound (orange) forms. The regions experiencing significant conformational changes upon OAA binding are highlighted in green, namely the $\alpha$-helical segment SRDDLIG (residues 88–94) in $\alpha 3$, which acts as the active-site door, and the GGHG loop (residues 174–177), which harbors the essential residue His176.

### 3.3. Mechanistic implications

By comparing the structures reported in this work, along with previous reports on a variety of lactate and malate dehydrogenases (Goward & Nicholls, 1994; Grau *et al.*, 1981; Hall & Banaszak, 1993; Hall *et al.*, 1992), the catalytic mechanism for MDH can be substantiated. The binding mode of $NAD^+$ in the *Mex*MDH–$NAD^+$ complex strongly suggests that the side chain of His176 is protonated and present as imidazolium, given the hydrogen-bonding pattern (Fig. 4). The amide protons of the $NAD^+$ carboxamide form hydrogen bonds to the backbone carbonyls of Met144 and Ile119. The proton at $N^{\delta 1}$ of His176 forms a hydrogen bond to Asp149, while the proton at $N^{\varepsilon 2}$ of His176 forms a hydrogen bond to the $NAD^+$ carboxamide carbonyl O atom. Upon substrate binding, His176 moves, maintaining the hydrogen bond with Asp149 and forming a new hydrogen bond between the proton at $N^{\varepsilon 2}$ and the C2 carbonyl O atom in oxaloacetate. Protonation of the C2 carbonyl O atom further polarizes the OAA carbonyl, facilitating hydride transfer from NADH. During

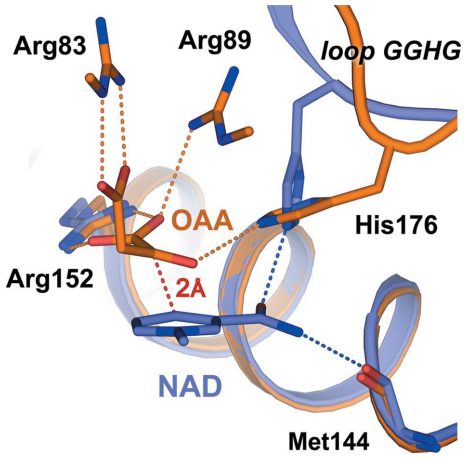


**Figure 4**
Secondary-structure matching superposition of $NAD^+$-bound (blue) and OAA-bound (orange) *Mex*MDH structures, suggesting the likely binding mode of OAA in the presence of NADH. Dashed lines indicate catalytically important hydrogen-bond interactions following the same color scheme, except for the red dashed line, which indicates the distance of 2 Å between the OAA carbonyl O atom and C4 of the nicotinamide ring holding the reactive hydride.

product formation His176 donates the proton from $N^{\varepsilon 2}$ to form the hydroxyl of (2*S*)-malate.

## 4. Concluding remarks

Here, we report the structure of *M. extorquens* malate dehydrogenase complexed with mechanistically relevant ligands. To our knowledge, this is the first report of a malate dehydrogenase that provides experimental, high-resolution atomic models supporting the well known reaction mechanism of $NAD^+$-dependent dehydrogenases belonging to the MDH/LDH-like superfamily.

## Funding information

This work was funded by Laboratory-Directed Research and Development-Directed Research grants (20130091DR and 20120776PRD4) from Los Alamos National Laboratory. Portions of this research were carried out at the Stanford Synchrotron Radiation Laboratory (SSRL), a national user facility operated by Stanford University on behalf of the US Department of Energy, Office of Basic Energy Sciences. The SSRL Structural Molecular Biology Program is supported by the Department of Energy, Office of Biological and Environmental Research, and by the NIH, National Center for Research Resources, Biomedical Technology Program and the National Institute of General Medical Sciences. Part of the research described in this paper was performed at the Canadian Light Source, which is supported by the Canada Foundation for Innovation, Natural Sciences and Engineering Research Council of Canada, the University of Saskatchewan, the Government of Saskatchewan, Western Economic Diversification Canada, the National Research Council Canada and the Canadian Institutes of Health Research.

## References

Anthony, C. (1982). *The Biochemistry of Methylotrophs.* London: Academic Press.
Bhat, T. N. (1988). *J. Appl. Cryst.* **21**, 279–281.
Chapman, A. D. M., Cortés, A., Dafforn, T. R., Clarke, A. R. & Brady, R. L. (1999). *J. Mol. Biol.* **285**, 703–712.
Cohen, A. E., Ellis, P. J., Miller, M. D., Deacon, A. M. & Phizackerley, R. P. (2002). *J. Appl. Cryst.* **35**, 720–726.
Colowick, S. P. & Kaplan, N. O. (1957). *Methods Enzymol.* **4**, 840–855.
Dalziel, K. (1962*a*). *Biochem. J.* **84**, 240–244.
Dalziel, K. (1962*b*). *Nature (London)*, **195**, 384–385.
Do, C. B., Mahabhashyam, M. S. P., Brudno, M. & Batzoglou, S. (2005). *Genome Res.* **15**, 330–340.
Emsley, P., Lohkamp, B., Scott, W. G. & Cowtan, K. (2010). *Acta Cryst.* D**66**, 486–501.
Evans, P. (2006). *Acta Cryst.* D**62**, 72–82.
Evans, P. R. & Murshudov, G. N. (2013). *Acta Cryst.* D**69**, 1204–1214.
French, S. & Wilson, K. (1978). *Acta Cryst.* A**34**, 517–525.
Goward, C. R. & Nicholls, D. J. (1994). *Protein Sci.* **3**, 1883–1888.
Grau, U. M., Trommer, W. E. & Rossmann, M. G. (1981). *J. Mol. Biol.* **151**, 289–307.
Hall, M. D. & Banaszak, L. J. (1993). *J. Mol. Biol.* **232**, 213–222.
Hall, M. D., Levitt, D. G. & Banaszak, L. J. (1992). *J. Mol. Biol.* **226**, 867–882.
Holm, L. & Rosenström, P. (2010). *Nucleic Acids Res.* **38**, W545–W549.
Kabsch, W. (2010). *Acta Cryst.* D**66**, 133–144.
Liebschner, D., Afonine, P. V., Moriarty, N. W., Poon, B. K., Sobolev, O. V., Terwilliger, T. C. & Adams, P. D. (2017). *Acta Cryst.* D**73**, 148–157.
Marchler-Bauer, A. *et al.* (2017). *Nucleic Acids Res.* **45**, D200–D203.
McCoy, A. J., Grosse-Kunstleve, R. W., Adams, P. D., Winn, M. D., Storoni, L. C. & Read, R. J. (2007). *J. Appl. Cryst.* **40**, 658–674.
Miller, M. A., Pfeiffer, W. & Schwartz, T. (2010). In *2010 Gateway Computing Environments Workshop (GCE)*. Piscataway: IEEE. https://doi.org/10.1109/GCE.2010.5676129.
Murshudov, G. N., Skubák, P., Lebedev, A. A., Pannu, N. S., Steiner, R. A., Nicholls, R. A., Winn, M. D., Long, F. & Vagin, A. A. (2011). *Acta Cryst.* D**67**, 355–367.
Rao, S. T. & Rossmann, M. G. (1973). *J. Mol. Biol.* **76**, 241–256.
Rozova, O., Khmelenina, V., Bocharova, K., Mustakhimov, I. & Trotsenko, Y. (2015). *Microorganisms*, **3**, 47–59.
Soltis, S. M. *et al.* (2008). *Acta Cryst.* D**64**, 1210–1221.
Stamatakis, A. (2014). *Bioinformatics*, **30**, 1312–1313.
Takahashi-Íñiguez, T., Aburto-Rodríguez, N., Vilchis-González, A. L. & Flores, M. E. (2016). *J. Zhejiang Univ. Sci. B*, **17**, 247–261.
The UniProt Consortium (2017). *Nucleic Acids Res.* **45**, D158–D169.
Vaguine, A. A., Richelle, J. & Wodak, S. J. (1999). *Acta Cryst.* D**55**, 191–205.
Waterhouse, A. M., Procter, J. B., Martin, D. M. A., Clamp, M. & Barton, G. J. (2009). *Bioinformatics*, **25**, 1189–1191.
Winn, M. D. *et al.* (2011). *Acta Cryst.* D**67**, 235–242.
Zarzycki, J. & Kerfeld, C. A. (2013). *BMC Struct. Biol.* **13**, 28.

STRUCTURAL BIOLOGY COMMUNICATIONS

ISSN: 2053-230X

# ORDER FORM

YOU WILL AUTOMATICALLY BE SENT DETAILS OF HOW TO DOWNLOAD AN ELECTRONIC REPRINT OF YOUR PAPER, FREE OF CHARGE. PRINTED REPRINTS MAY BE PURCHASED USING THIS FORM.

Please scan your order and send to lj@iucr.org

**INTERNATIONAL UNION OF CRYSTALLOGRAPHY**
5 Abbey Square
Chester CH1 2HU, England.

VAT No. GB 161 9034 76

Article No.: F181180-RF5009

Title of article Conformational changes on substrate binding revealed by structures of *Methylobacterium extorquens* malate dehydrogenase

Name Clifford J. Unkefer

Address Bioscience Division, Los Alamos National Laboratory, Los Alamos, NM 87544, USA

E-mail address (for electronic reprints) cju@lanl.gov

## OPEN ACCESS

IUCr journals offer authors the chance to make their articles open access on **Crystallography Journals Online**. For full details of our open-access policy, see http://journals.iucr.org/services/openaccess.html. For authors in European Union countries, VAT will be added to the open-access charge.

If you wish to make your article open access please go to http://shop.iucr.org/iucrshop/viewitem/openaccess/?code=RF5009 The charge for making an article open access is **1100 United States dollars**.

## DIGITAL PRINTED REPRINTS

I wish to order . . . . . paid reprints

**These reprints will be sent to the address given above. If the above address or e-mail address is not correct, please indicate an alternative:**

## PAYMENT (REPRINTS ONLY)

Charge for reprints . . . . . USD

☐ An official purchase order made out to **INTERNATIONAL UNION OF CRYSTALLOGRAPHY** ☐ is enclosed ☐ will follow

Purchase order No.

☐ Please invoice me

☐ I wish to pay by credit card

*EU authors only*: VAT No:

Date | Signature

## OPEN ACCESS

The charge for making an article open access is **1100 United States dollars**. For authors in European Union countries, VAT will be added to the open-access charge.

A paper may be made open access at any time after the proof stage on receipt of the appropriate payment. This includes all back articles on **Crystallography Journals Online**. For further details, please contact support@iucr.org. Likewise, organizations wishing to sponsor open-access publication of a series of articles or complete journal issues should contact support@iucr.org.

## DIGITAL PRINTED REPRINTS

An electronic reprint is supplied free of charge.

Printed reprints without limit of number may be purchased at the prices given in the table below. The requirements of all joint authors, if any, and of their laboratories should be included in a single order, specifically ordered on the form overleaf. All orders for reprints must be submitted promptly.

Prices for reprints are given below in **United States dollars** and include postage.

| | Size of paper (in printed pages) | | | | |
|---|---|---|---|---|---|
| Number of reprints required | 1–2 | 3–4 | 5–8 | 9–16 | Additional 8's |
| 50 | 184 | 268 | 372 | 560 | 246 |
| 100 | 278 | 402 | 556 | 842 | 370 |
| 150 | 368 | 534 | 740 | 1122 | 490 |
| 200 | 456 | 664 | 920 | 1400 | 610 |
| Additional 50's | 86 | 128 | 178 | 276 | 116 |

## PAYMENT AND ORDERING

Open-access fees should be paid at http://shop.iucr.org/iucrshop/viewitem/openaccess/?code=RF5009

Official purchase orders should be made out to **INTERNATIONAL UNION OF CRYSTALLOGRAPHY**.

Orders should be returned by email to lj@iucr.org

## ENQUIRIES

Enquiries concerning reprints should be sent to support@iucr.org.